Strut and texture analysis for osteoporosis detection index (ODI) using dental panoramic radiography

Jae Joon Hwang

The Graduate School

Yonsei University

Department of Dentistry

Strut and texture analysis for osteoporosis detection index (ODI) using dental panoramic radiography

Directed by Professor Sang-Sun Han, D.D.S., Ph.D.

The Doctoral Dissertation submitted to the Department of Dentistry, and the Graduate School of Yonsei University in partial fulfillment of the requirements for the degree of Doctor of Philosophy

Jae Joon Hwang

December 2016

This certifies that the Doctoral Dissertation of

Jae Joon Hwang is approved.

Thesis Supervisor: **Prof. Sang-Sun Han**

Thesis Committee Member: **Prof. Jinna Kim**

Thesis Committee Member: **Prof. Hyun Sil Kim**

Thesis Committee Member: **Prof. Yoon Jeong Choi**

Thesis Committee Member: **Prof. Ho-Gul Jeong**

The Graduate School

Yonsei University

December 2016

Acknowledgement

First and foremost, I would like to express my special appreciation to my advisor Professor Sang-Sun Han for the continuous support of my study and related research. Your patience, motivation, immense knowledge and guidance helped me in all the time of research and writing of this thesis.

Besides my advisor, I would like to thank the rest of my thesis committee. Prof. Jinna Kim, Prof. Hyun Sil Kim, Prof. Yoon Jeong Choi, and Prof. Ho-Gul Jeong for their insightful comments and encouragement, but also for the hard question which incented me to widen my research from various perspectives.

Also I am really thankful to Jeong-Hee Lee for the precise vision, stimulating discussions and collaborations. Without that precious support it would not be possible to conduct this research. My sincere thanks also goes to our research partner Young Hyun Kim for gaining necessary data in the research facilities.

Last but not the least, I would like to express my sincere gratitude to my family. My mother and sister who cheer me up when in great need of inspiration and my father who always takes care of my health. In the end, Yonsei University was the exceptional scientific research experience and extraordinary memory of my lifetime.

December, 2016

Jae Joon Hwang

TABLE OF CONTENTS

LIST OF FIGURES

LIST OF TABLES

Abstract

Strut and texture analysis for osteoporosis detection index (ODI) using dental panoramic radiography

Jae Joon Hwang

Department of Dentistry
The Graduate School, Yonsei University

(Directed by Professor Sang-Sun Han, D.D.S., Ph.D.)

Together with rapid aging of worldwide population, prediction and early diagnosis of osteoporosis became an important health care issue. The aim of this study was to find variables for enabling osteoporosis detection using the strut method, fractal dimension (FD), and the gray level co-occurrence matrix (GLCM) in dental panoramic radiographs (DPRs) using multiple ROIs (regions of interests), including the endosteal margin area, and to develop an osteoporosis detection index (ODI) applicable to DPRs.

A total of 454 DPRs from 2012 to 2015 were selected, with 227 drawn from non-osteoporotic patients and 227 drawn from osteoporotic patients, classified by bone mineral density (T-score). After 3 marrow regions and the endosteal margin area were upsampled to 400%, strut features, FD, and GLCM were analyzed using a customized image processing program. Independent samples t-test was used to verify statistical differences between the normal and osteoporotic

patients. Logistic regression was performed to compare the diagnostic accuracy of each variable. Finally, decision tree algorithm was used to create and verify the ODI.

FD (0.975) and strut features (below 0.926) of the endosteal margin area showed high area under the curve (AUC), whereas GLCM (below 0.580) showed low AUC. The combination of FD and two strut features (number of nodes denominated by number of termini, and number of nodes per square centimeter) showed a high diagnostic accuracy (93.0%) with use of the decision tree.

This combination of FD and two strut features in endosteal margin area showed potential as an ODI to be used with DPRs.

Keywords : Fractals; Image processing, Computer-Assisted; Mandible; Osteoporosis; Panoramic; Radiography

Strut and texture analysis for osteoporosis detection index (ODI) using dental panoramic radiography

Jae Joon Hwang

Department of Dentistry
The Graduate School, Yonsei University

(Directed by Professor Sang-Sun Han, D.D.S., Ph.D.)

I. INTRODUCTION

Osteoporosis is characterized by low bone mass and micro-architectural deterioration.[1] This is the result of net bone loss which is caused by accelerated osteoclastic resorption breaking down the orchestrated balance between bone resorption and formation.[2] This disease is referred to as a silent bone disorder associated with fragility fractures since a significant number of osteoporotic cases go undiagnosed until the first bone fracture.[3] The most common fracture sites are the hip, spine, and wrist. Hip fractures are especially devastating because they are associated with loss of function and high mortality. In 1990 over 1.2 million hip fractures occurred worldwide. This number is expected to grow to 2.6 million by 2025.[4] With the rapid aging of the worldwide population, the prediction and early diagnosis of osteoporosis has become an important health care issue.[5,6]

The current principal method for diagnosing osteoporosis is bone mineral density (BMD).[7] Osteoporosis has been defined by the World Health Organization as a T-score that is 2.5 standard deviations below the young normal mean. BMD is usually measured using dual energy X-ray absorptiometry (DXA). The use of a dual-energy beam enables the measurement of bone density alone by subtracting the effect of soft tissue.[8,9] Since this technique is expensive and requires certified X-ray technicians, it is not used for all patients regularly. Therefore, it is necessary to develop a low-cost and convenient tool for screening patients who have an indication for DXA.

Reduced bone mass of the jaw is also a consequence of osteoporosis in the oral and maxillofacial region. The mandibular mineral content is reduced in subjects with osteoporotic fractures.[8] Further, reductions in cortical and subcortical alveolar bone density have also been found to be correlated with osteoporosis in longitudinal studies.[10,11] Endosteal bone resorption in association with osteoporosis is well known in the skeleton.[12] Additionally, radiographic erosive changes of mandibular endosteal margin in osteoporotic patients have been constantly reported.[13,14]

Since dental panoramic radiographs (DPRs) can provide a valuable screening opportunity and their cost is included in routine dental care, many studies have discussed the use of the DPRs for the identification of low skeletal BMD.[15-17] Loss of bone density in osteoporotic patients has been found in routine oral exams using DPRs.[18]

The most commonly studied region of interest (ROI) for osteoporosis detection is the inferior cortex in DPRs. The thickness of the inferior cortex of the mandible below the mental foramen has been measured directly (mandibular cortical width, MCW) or as a ratio of the thickness divided by the distance from the mental foramen to the inferior border (panoramic mandibular index, PMI).[13,14,19] The inferior cortex tends to be thinner in osteoporotic patients, although some studies have not confirmed this relationship. This thickness in DPRs can be changed by the head position of the subject. Erosions of the inferior cortex are typically classified into 3 groups by using the mandibular cortical index (MCI). Patients with osteoporosis are also more likely to show erosions of the inferior cortex than controls.[13,14,19] However, the MCI has the limitation of a lack of complete reproducibility, which is associated with visual assessment.

A number of efforts have been made to overcome this lack of reproducibility by using objective analytical methods to screen for osteoporosis in DPRs. Texture analysis such as fractal dimension (FD) and the gray level co-occurrence matrix (GLCM) are have been used in such efforts.[15,20-24] Morphometric analysis, such as the strut method, has been applied to the ramus area in DPRs.[25] However, these methods have provided conflicting results, and efforts to find an index that provides a simple threshold for detecting osteoporosis in DPRs are still ongoing now. One reason for these different results might be use of the ROIs such as the marrow and the inferior cortex, which might show less noticeable features in osteoporotic

patients. Another reason may be differences in image processing methods. Many studies used the binarization method described by White et al.[4,7,26] for calculating FD. However, these studies used different parameter settings for density correction during the process.

In this study, the endosteal margin area was adopted as new ROI. This area, which includes both the inferior cortex and the marrow enclosing the endosteal margin, was used as part of an objective analysis to capture the pattern change around the margin, which has been addressed in MCW and MCI studies. Previous studies analyzed each the inferior cortex and marrow separately, unlike this study, which focused on the entirety of the adjacent area. The strut method was also newly adopted for the analysis of the endosteal margin area in this study. This method has been most commonly applied to intraoral radiography in dentistry for analyzing trabecular bone patterns. We expected strut analysis to capture the degree of erosive change in the endosteal margin area. A combination of morphometric and texture analysis was tried in multiple ROIs, including the endosteal margin area as well as the marrow area of DPRs, for the first time in this study. In order to ensure reproducible image processing, parameter adjustment was performed before the experiment for adequate density correction.

The purposes of this study were (1) to find variables enabling osteoporosis detection using the strut method, FD, and GLCM in DPRs with multiple ROIs including the endosteal margin area and (2) to develop an osteoporosis detection

index (ODI) to be used with DPRs.

II. MATERIALS AND METHODS

1. Subjects

454 DPRs (227 from normal patients, and 227 from patients with osteoporosis; Table 1) with T-scores from 2012 to 2015 taken for oral examinations in Yonsei university dental hospital were used for the analysis. Patients with a T-score below -2.5 for at least 1 site among the lumber spine vertebrae 1-4, the femur neck, trochanter, total hip, and Ward's triangle were defined as having osteoporosis, while patients with a T-score above -1.0 at all of these locations defined as normal. Patients taking drugs to treat osteoporosis were excluded from this study. Basic demographic information and T-scores are listed in Table 1. A Cranex 3+ Ceph panoramic dental X-ray (Soredex Co, Helsinki, Finland) was used with voltage settings of 67-71 kV at 10 mA (exposure time, 19.5 seconds). All images were taken by a skilled technician according to a standard protocol following the manufacturer's instructions, with patients' occlusal plane parallel to the floor and the center of the focal trough fitted to the patients' canine. These images were stored according to Digital Images in Communication and Medicine (DICOM) 3.0 in a medical image file format (512×512 pixels) on a Windows 7-based graphics workstation (Intel Core i5 3570, 4 GByte, calibrated 21.3-inch color monitor, resolution of 1563×2048 pixels, NVIDIA Quadro 2000 graphics card) and subsequently transferred to MATLAB R2016a (MathWorks, Natick, MA, USA). All images were normalized in the range 0.0 (black) to 1.0 (white). A radiologist

with more than 4-years of experience then selected images suitable for the inclusion criteria, selecting images with no blurring, motion artifacts, surgical defects, or overlapping hyoid bone.

Table 1. Differences in mean values of age and bone mineral density between osteoporotic and normal patients.

Variables	Osteoporosis (n=227)	Normal (n=227)	Total (n=454)
Male (n) (%)	34 (15.0)	61 (26.9)	95 (20.9)
Female (n) (%)	193 (85.0)	166 (73.1)	359 (79.1)
Age*	64.44 (12.96)	57.49 (11.93)	60.96 (12.92)
BMD			
L1-L4 (g/cm^2)	-1.60 (2.20)	0.08 (0.99)	-0.75 (1.90)
Femur neck (g/cm2)	-1.40 (1.88)	-0.13 (0.70)	-0.77 (1.56)
Trochanter (g/cm^2)	-0.89 (1.43)	0.42 (0.84)	-0.24 (1.35)
Total hip (g/cm^2)	-0.97 (1.49)	0.45 (0.77)	-0.27 (1.38)
Ward's (g/cm^2)	-1.90 (2.43)	-0.39 (0.99)	-1.16 (2.01)

The given values are means, and values between brackets indicate the standard deviation.

*Mean age refers to the age of subjects at the time of the radiographic imaging.

Abbreviations: BMD, bone mineral density.

2. Measurements

Custom analysis program

Using MIJ version 1.3.9 (Biomedical Imaging Group) which is a Java package for exchanging images between MATLAB (R2016a, MathWorks, Natick, MA, USA) and ImageJ (version 1.6; National Institutes of Health, Bethesda, MD, USA), we

made a customized computer program including functionalities of ROI selection and feature analysis.

Four ROIs were selected consecutively according to the instructions of the program (Fig 1, Table 2). The side of the bilateral region with less noise and fewer overlapping structures were selected as an ROI. For ROIs 1-3, a fixed square dimension (5 mm × 5 mm) was selected, the size of which was determined experimentally as not including contact with the root or adjacent cortical layer. For ROI 4, after an observer defined several points along the endosteal margin from the anterior margin of the ramus to the midpoint between the central line of the DPRs and anterior margin of the ramus, the program automatically connected the points with smooth spline curves. Then a curved ROI, containing margins 3 mm above and below this spline curve, was generated and stretched in a rectangular shape. Since variations were present in the height of the inferior cortex in the stretched image, the final ROI height was refined manually to avoid contact with the inferior margin of the cortex (Fig 2E).

After localizing the ROIs, this program adjusted the image and filter parameter size in a preliminary examination following the condition that medium and fine structures were well represented in the binary image. The image was resized to 400% with using bicubic interpolation (upsampling, Fig 3) and the parameters of a Gaussian filter were set to a sigma value of 35 and a filter size of 33. In order to preserve detailed structures during binarization, blurring is necessary with a

Gaussian filter to remove large-scale gray level variations in the image. Such variations have various causes, such as image noise, the presence of overlapping soft tissue, and differences in the thickness of the object. The density correction step removes these large-scale variations and adjusts the density of the image by blurring the ROI and subtracting the blurred image from the original one.[26] The binarization process was followed. The effect of upsampling with the adjusted parameter setting is shown in Figure 4.

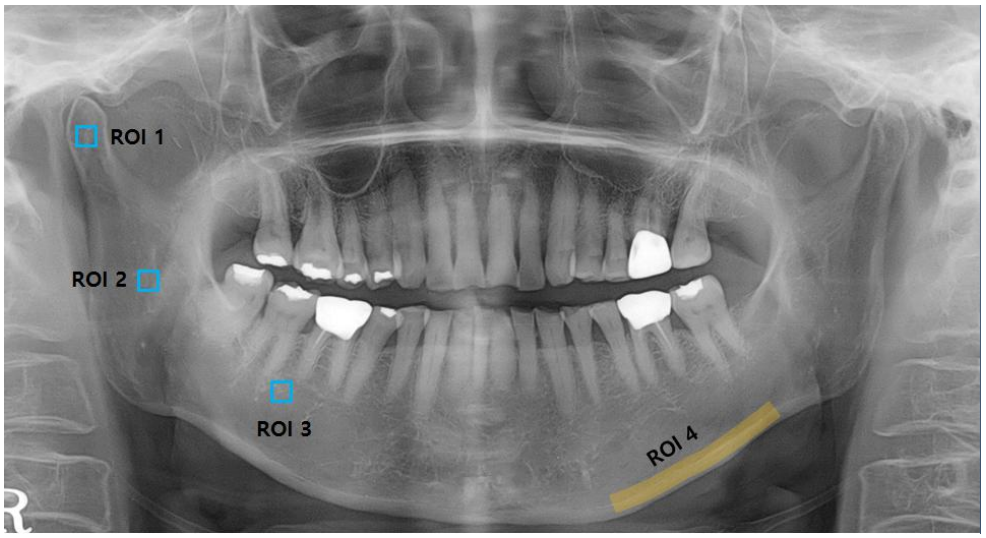

Figure 1. A total 4 regions of interest (ROIs) were selected in the DPR analysis: center of condylar head (ROI 1), center of the ramus (ROI 2), and medulla below and between 2 molars (ROI 3). If a molar was missing, the area 2 cm medial from the anterior margin of the ramus was selected. The endosteal margin area (ROI 4) was selected from anterior margin of the ramus to the midpoint between the center line of the DPRs and the anterior margin of the ramus.

Table 2. Four ROIs used in DPRs analysis.

ROI	Size	Definition
ROI 1	5 mm x 5 mm	Center of condyle head
ROI 2	〃	Center of ramus
ROI 3	〃	Area below and between two molars
ROI 4	User defined	Endosteal margin area from anterior margin of the ramus to the midpoint between the center line of DPRs and anterior margin of the ramus

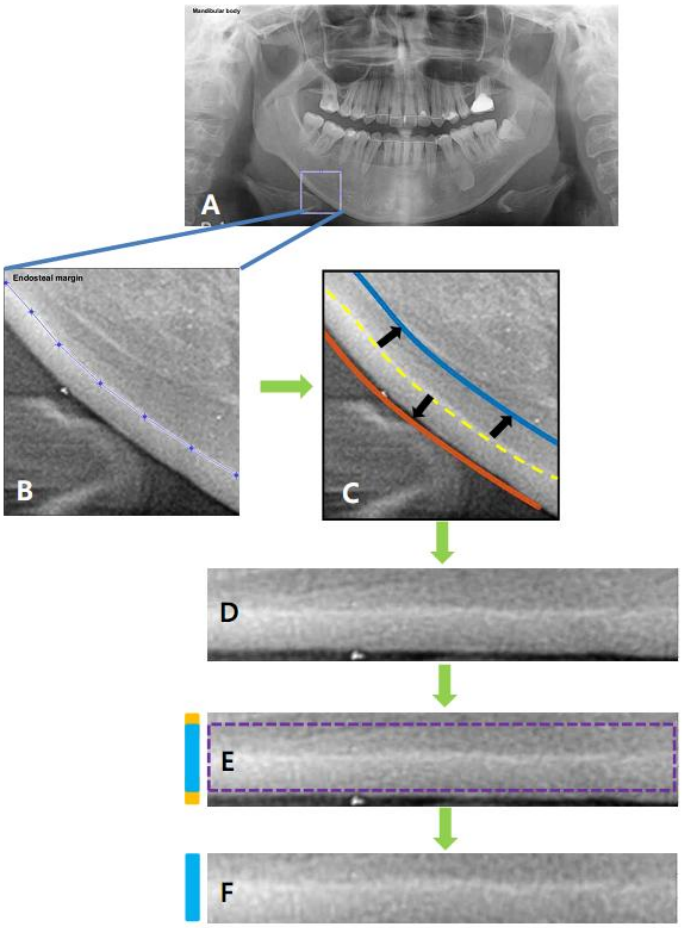

Figure 2. Regions of interest (ROI) 4 (the endosteal margin area) was selected by a customized program using the 5 steps below.

A. ROI containing endosteal margin area; B. User defined points along the endosteal margin; C. Smooth spline (yellow dotted curve) connecting the user-defined points and curved ROI 3mm above (blue curve) and below (orange curve) the spline curve; D. Stretched rectangular ROI; E. Redefined ROI not touching the inferior border; the dotted purple line represents the redefined ROI, the blue bar represents the maximum length not touching the inferior border, and the yellow bar represents the length below the inferior border; F. Final ROI with upper and lower boundaries trimmed.

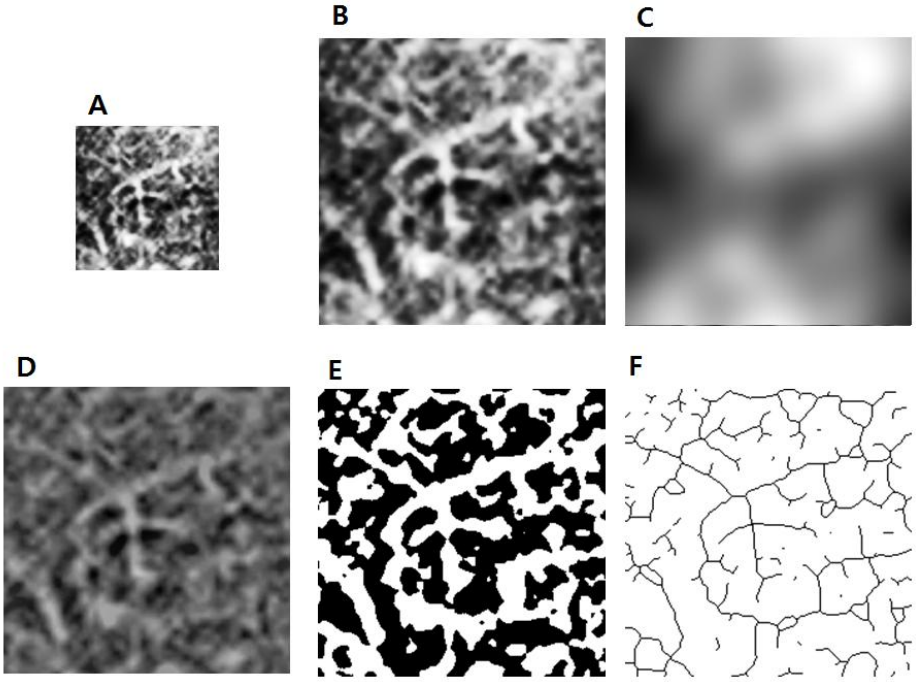

Figure 3. Steps used in image processing. A, Original image; B, Upsampled image; C, Blurred image; D, Subtracted image (B-C); E, Binary image made of D; F, Skeletonized image made of D.

Strut analysis

Area of high density and the length of the periphery were analyzed using a binary image. The high-density region was defined as representing white pixels in the binary image. The periphery corresponded to the outer margin of the high-density region. Skeletonization of the binary image was performed for analyzing structural elements (Fig 3F), which consist of a node (crossing point), terminus (free end), and strut (connection between two other elements) (Fig 5). In the analysis, the number of termini and nodes, as well as the number and length of struts, were calculated.

All features were expressed as a proportion of the related length, area, or perimeter to facilitate direct comparison (Table 3).

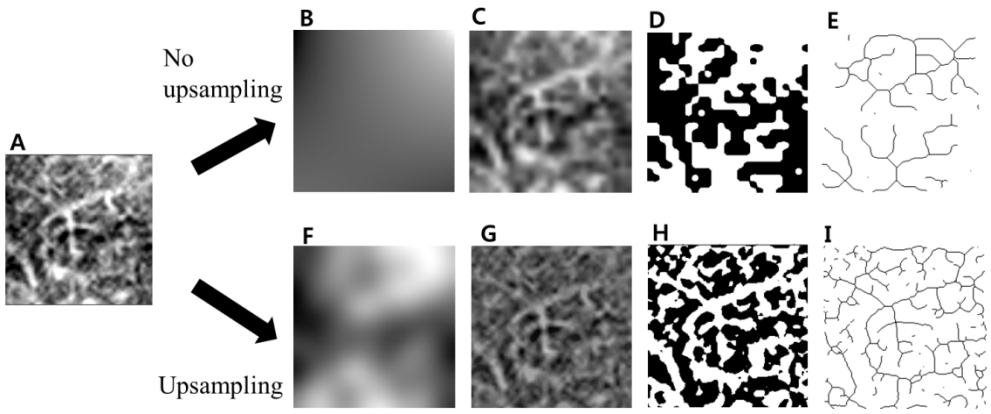

Figure 4. Image processing results according to different upsampling (resizing with interpolation) under a Gaussian filter of a sigma value of 35, and a filter size of 33. When resampled to 400%, the image showed detailed structures in the binary and skeletonized output.
A. Original image (5 mm × 5 mm); B-E. Processed using original image size; F-I. Processed using upsampled image; B, F. Blurred image; C, G. Density corrected image (original image minus the blurred image); D, H. Binary image; E, I. Skeletonized image.

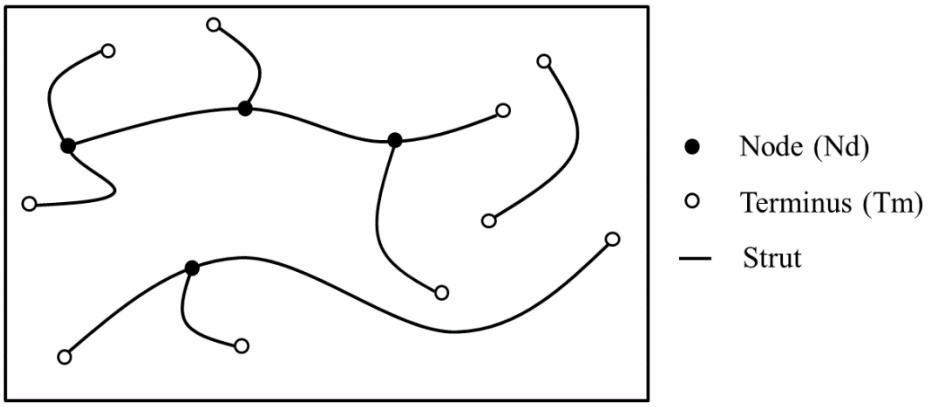

Figure 5. The schema of strut analysis which comprises nodes, termini, and struts.

Table 3. Description of features used in this study.

Features	Description
FD	Statistical index of complexity comparing how detail in a pattern changes with the scale at which it is measured
Strut	
HDA/total area	Area of high density region denominated by total area of the ROI
Periphery/total area	Periphery denominated by total area
Periphery/HDA	Periphery denominated by area of high density region
TSL/HDA	Total strut length denominated by area of high density region
TSL/total area	Total strut length denominated by total area
N.Tm/sq cm	Number of termini per square centimeter
N.Tm/TSL	Number of termini denominated by total strut length
N.Tm/periphery	Number of termini denominated by periphery
N.Tm/HDA	Number of termini denominated by area of high density region
N.Nd/sq cm	Number of nodes per square centimeter
N.Nd/TSL	Number of nodes denominated by total strut length
N.Nd/periphery	Number of nodes denominated by periphery
N.Nd/HDA	Number of nodes denominated by are of high density region
N.Nd/N.Tm	Number of nodes denominated by number of terminus
GLCM	
Contrast	Measures the intensity contrast between pixel and its neighbor over the whole image.
Correlation	Measures the joint occurrence probability of the specified pixel pairs over the whole image.
Energy	Provides the sum of squared elements.
Homogeneity	Measures the closeness of the distribution of elements in the GLCM to the GLCM diagonal.

Abbreviations: HDA, area of a high-density region; Periphery, the total number of pixels on the outer margin of the high-density region; TSL, total length of struts; N, number; Tm, Termini; Nd, Nodes; sq, square.

Fractal dimension (FD)

FD is the most commonly used texture investigation method in screening for osteoporosis.[24] An FD is a ratio providing a statistical index of complexity comparing how the detail in a pattern changes with the scale at which it is measured. The higher the FD is, the more irregular the perimeter of the object. Many studies have attempted to apply FD to DPRs for detecting bone pattern changes in osteoporotic patients. FD in this study was calculated using binary images and the box-counting method [22] as follows:

FD = 1- [Log (number of occupied boxes) versus Log (length of box side)]

GLCM features

GLCM is a way of analyzing texture features using a second-order statistic that can be used to describe the spatial distribution of the gray levels in an image in terms of local variation, homogeneity, and correlation of pixels in the image.[24] Unlike the strut method and FD, GLCM uses an original image because GLCM processes the gray level as part of the calculation. In this study, the following 4 textural features were calculated from each ROI: contrast, correlation, energy, and homogeneity (Table 3).

3. Statistical analysis

The paired sample *t*-test was used to assess intra-observer and inter-observer reliability for ROI selection. The second measurement was performed by 2 observers 2 weeks after the first measurement, using the same 20 DPRs.

We compared the variables of the 2 groups using the independent samples *t*-test. The area under the curve (AUC) was calculated using the receiver operating characteristic (ROC) curve based on logistic regression to compare the performance of each variable for detecting osteoporosis. The highest sensitivity and specificity values were obtained based on the best cut-off point for AUC.

The decision tree algorithm was also used to create a predictive classification model to develop an index (ODI) for osteoporosis detection in DPRs. A 10-fold cross validation was performed to validate the accuracy of the model. We used the chi-squared automatic interaction detection (CHAID) for the decision tree algorithm in R (PARTY). All statistical tests were conducted using R statistical software version 3.3.1 (R Development Core Team, Cambridge, MA, USA). The tests were 2-sided and $p<0.05$ was considered the cut-off for statistical significance.

III. RESULTS

No significant differences were found in inter-observer and intra-observer reliability (0.051-0.942) of 95% of the variables in the 4 ROIs. The endosteal margin area (ROI 4) showed discriminating features in the image processing results (Fig 6). Binary and skeletonized images of osteoporotic patients tended to show longer and more connected structures than were observed in the normal group. Table 4 presents summary statistics regarding the strut and textural features in the 4 ROIs.

ROI 4 showed significant differences for 16 strut features out of the total of 19 (Table 4, Fig 7). However, the number of termini per periphery (N.Tm/periphery), correlation, and energy showed no significant differences. Osteoporotic patients showed significantly higher values for FD, the area of the high-density region, total strut length, and periphery length in this ROI. Features related to termini also showed an increase, whereas features related to nodes exhibited showed a reduction. Homogeneity was slightly lower, whereas contrast was higher in osteoporotic patients. A box plot was used to present the greatest differences in FD, number of nodes per number of termini (N.Nd/N.Tm), and periphery as a ratio of the total area (Periphery/total area) between osteoporotic and normal patients in this ROI (Fig 8).

Only 7 variables showed statistical significance in the other 3 ROIs. This was the case for N.Nd/N.Tm and the number of nodes per total strut length (N.Nd/TSL) in the center of the condyle (ROI 1); contrast, correlation, and homogeneity in the

center of the ramus (ROI 2); and periphery per total area (Periphery/total area) and periphery per high-density area (Periphery/HDA) below and between 2 molars (ROI 3).

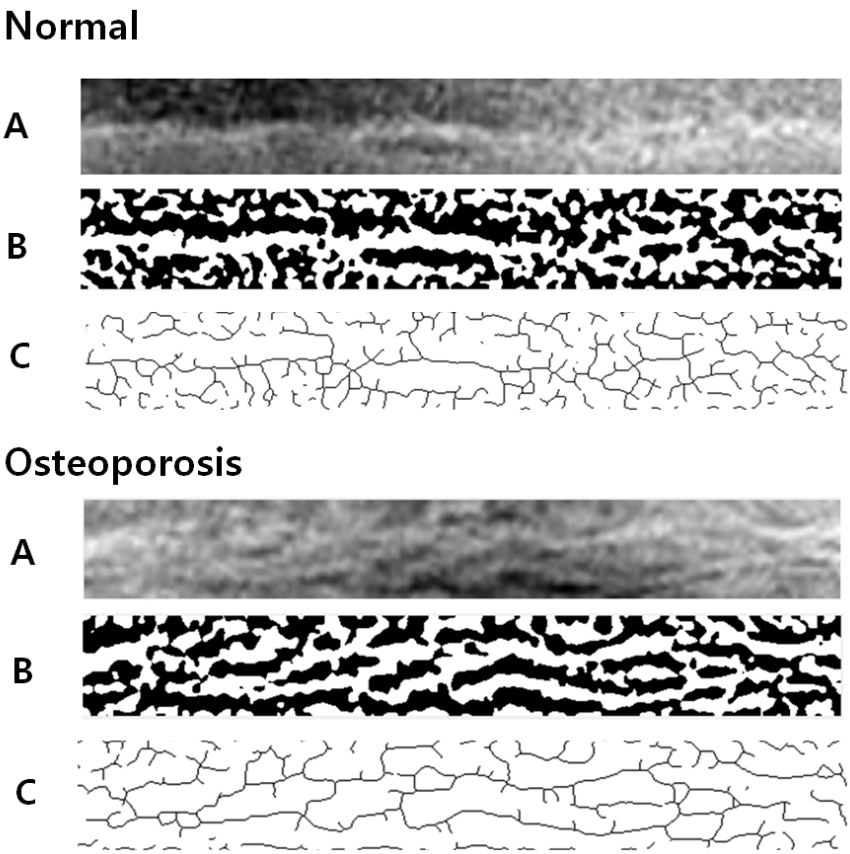

Figure 6. Processed images show the pattern difference between normal and osteoporotic patients. The image processing results shows the different patterns in normal and osteoporotic patients. The binary and skeletonized images of osteoporotic patients show longer and more connected structures than found in the normal group.

A. Original image; B. Binary image; C. Skeletonized image.

Table 4. Mean and standard deviation for textural feature of the osteoporotic and normal patients.

Textural feature	ROI 1			ROI 2		
	Osteoporosis (Mean ± SD)	Normal (Mean ± SD)	*P* value	Osteoporosis (Mean ± SD)	Normal (Mean ± SD)	*P* value
Fractal dimension (FD)	1.271 ± 0.063	1.275 ± 0.071	0.460	1.290 ± 0.071	1.289 ± 0.075	0.819
Strut						
HDA/total area	0.490 ± 0.017	0.491 ± 0.020	0.366	0.482 ± 0.020	0.483 ± 0.019	0.499
Periphery/total area	0.074 ± 0.006	0.073 ± 0.007	0.148	0.077 ± 0.007	0.076 ± 0.008	0.696
Periphery/HDA	0.151 ± 0.014	0.149 ± 0.017	0.136	0.159 ± 0.016	0.158 ± 0.019	0.575
TSL/HDA	0.081 ± 0.005	0.081 ± 0.006	0.940	0.084 ± 0.005	0.083 ± 0.006	0.864
TSL/total area	0.040 ± 0.003	0.040 ± 0.003	0.628	0.040 ± 0.003	0.040 ± 0.003	0.907
N.Tm/sq cm	120.007 ± 13.664	121.087 ± 15.816	0.437	126.935 ± 16.968	126.914 ± 17.758	0.990
N.Tm/TSL	30.452 ± 3.488	30.593 ± 3.651	0.675	31.617 ± 4.330	31.567 ± 4.319	0.901
N.Tm/periphery	16.341 ± 1.930	16.709 ± 2.214	0.060	16.624 ± 1.962	16.708 ± 2.089	0.660
N.Tm/HDA	2.455 ± 0.302	2.469 ± 0.340	0.632	2.639 ± 0.388	2.635 ± 0.414	0.900
N.Nd/sq cm	80.076 ± 13.317	78.06 ± 13.647	0.112	81.210 ± 12.867	82.047 ± 15.666	0.534
N.Nd/TSL	20.183 ± 2.498	19.585 ± 2.335	0.009*	20.077 ± 2.208	20.229 ± 2.816	0.523
N.Nd/periphery	10.907 ± 1.870	10.774 ± 1.919	0.454	10.651 ± 1.698	10.828 ± 2.146	0.331
N.Nd/HDA	1.634 ± 0.260	1.588 ± 0.263	0.061	1.682 ± 0.244	1.696 ± 0.309	0.598
N.Nd/N.Tm	0.673 ± 0.122	0.649 ± 0.109	0.029*	0.648 ± 0.118	0.654 ± 0.133	0.575
Grey-level co-occurrence matrix features (GLCM)						
Contrast	0.228 ± 0.053	0.226 ± 0.053	0.759	0.226 ± 0.062	0.211 ± 0.061	0.009*
Correlation	0.942 ± 0.017	0.944 ± 0.016	0.395	0.941 ± 0.019	0.946 ± 0.002	0.001*
Energy	0.103 ± 0.014	0.104 ± 0.017	0.704	0.109 ± 0.022	0.110 ± 0.019	0.669
Homogeneity	0.844 ± 0.034	0.844 ± 0.032	0.959	0.847 ± 0.039	0.856 ± 0.039	0.015*

continue on next page

Textural feature	ROI 3			ROI 4		
	Osteoporosis (Mean ± SD)	Normal (Mean ± SD)	*P* value	Osteoporosis (Mean ± SD)	Normal (Mean ± SD)	*P* value
Fractal dimension (FD)	1.225 ± 0.070	1.217 ± 0.067	0.187	1.065 ± 0.008	1.049 ± 0.004	<0.001*
Strut						
HDA/total area	0.482 ± 0.018	0.483 ± 0.019	0.656	0.468 ± 0.012	0.463 ± 0.009	<0.001*
Periphery/total area	0.070 ± 0.007	0.069 ± 0.007	0.023*	0.106 ± 0.007	0.096 ± 0.004	<0.001*
Periphery/HDA	0.146 ± 0.016	0.143 ± 0.016	0.031*	0.227 ± 0.017	0.208 ± 0.010	<0.001*
TSL/HDA	0.076 ± 0.007	0.074 ± 0.007	0.054	0.111 ± 0.007	0.104 ± 0.004	<0.001*
TSL/total area	0.036 ± 0.003	0.036 ± 0.003	0.095	0.052 ± 0.003	0.048 ± 0.002	<0.001*
N.Tm/sq cm	107.148 ± 19.113	106.47 ± 18.013	0.698	196.085 ± 33.221	176.72 ± 18.911	<0.001*
N.Tm/TSL	29.353 ± 4.276	29.68 ± 4.579	0.432	37.721 ± 5.314	36.715 ± 3.341	0.016*
N.Tm/periphery	15.186 ± 2.104	15.431 ± 2.073	0.212	18.388 ± 2.447	18.319 ± 1.673	0.726
N.Tm/HDA	2.230 ± 0.428	2.213 ± 0.408	0.663	4.204 ± 0.792	3.821 ± 0.463	<0.001*
N.Nd/sq cm	66.693 ± 15.342	65.145 ± 13.305	0.251	111.955 ± 21.317	120.901 ± 13.428	<0.001*
N.Nd/TSL	18.110 ± 2.979	17.994 ± 2.451	0.650	21.497 ± 3.311	25.084 ± 2.029	<0.001*
N.Nd/periphery	9.485 ± 2.122	9.455 ± 1.734	0.868	10.516 ± 1.789	12.539 ± 1.272	<0.001*
N.Nd/HDA	1.383 ± 0.312	1.349 ± 0.266	0.208	2.397 ± 0.480	2.612 ± 0.309	<0.001*
N.Nd/N.Tm	0.629 ± 0.134	0.620 ± 0.123	0.465	0.573 ± 0.065	0.685 ± 0.045	<0.001*
Grey-level co-occurrence matrix features (GLCM)						
Contrast	0.229 ± 0.034	0.228 ± 0.035	0.768	0.046 ± 0.010	0.043 ± 0.008	<0.001*
Correlation	0.943 ± 0.012	0.944 ± 0.012	0.783	0.991 ± 0.002	0.992 ± 0.002	0.081
Energy	0.104 ± 0.012	0.104 ± 0.014	0.882	0.141 ± 0.011	0.141 ± 0.009	0.798
Homogeneity	0.849 ± 0.023	0.848 ± 0.023	0.811	0.971 ± 0.006	0.972 ± 0.005	0.048*

Abbreviations: HDA, area of high-density region; Periphery, the total number of pixels on the outer margin of the high-density region; TSL, total length of struts; N, number; Tm, Termini; Nd, Nodes; sq, square.*P<0.05.

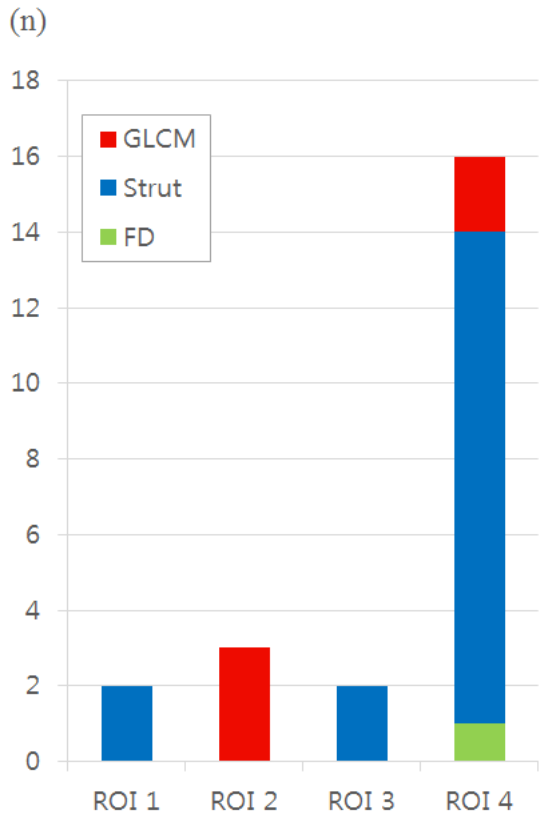

Figure 7. Number of variables of 3 analysis methods (FD, strut, and GLCM) which showed statistical significance in 4 ROIs.

(n) represents for number of variables which showed statistical significance.

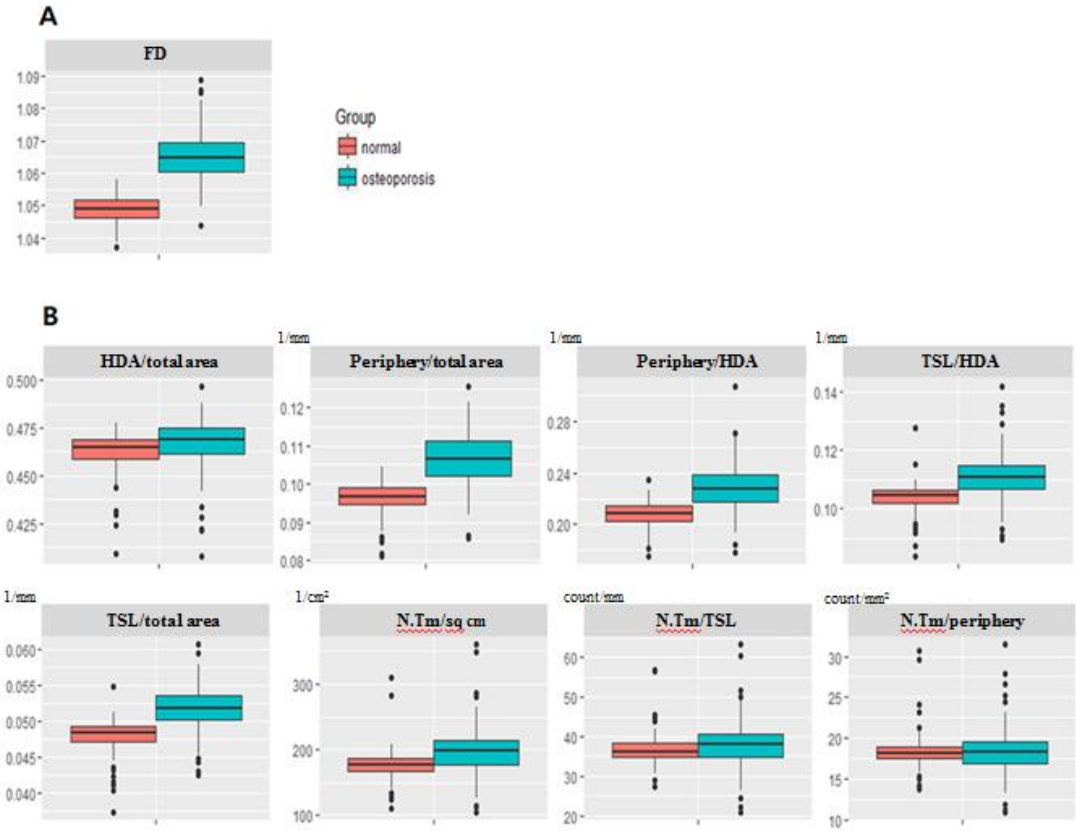

continue on next page

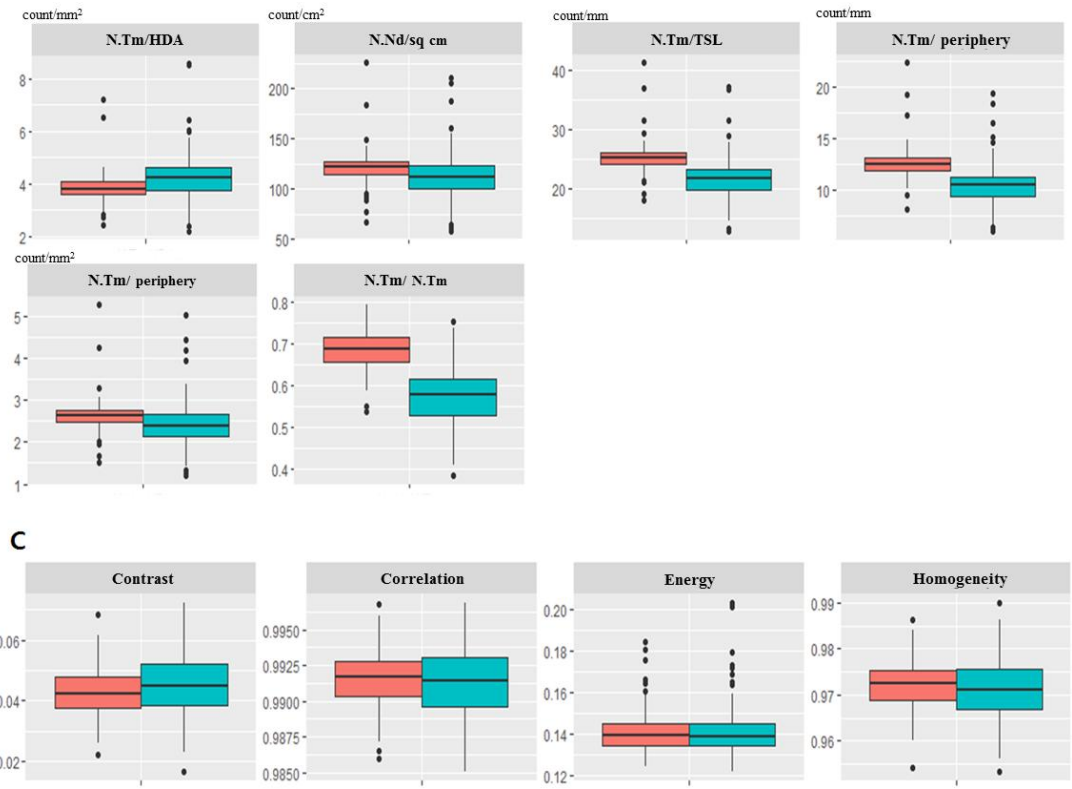

Figure 8. Differential presence of the strut and textural features between osteoporotic and normal patients in ROI 4.

A. FD; B. Strut method; C. GLCM.

By logistic regression, FD and N.Nd/N.Tm showed an excellent AUC (>0.9) for detecting osteoporosis, with values of 0.975 (95% confidence interval [CI]=0.962-0.987) and 0.926 (95% CI=0.901-0.950), respectively. Six other strut features showed a very good AUC (> 0.8). In contrast, the AUC of GLCM was low, ranging from 0.512 (95% CI=0.459-0.566) to 0.580 (95% CI=0.528-0.633) (Table 5). ROC curves for N.Nd/N.Tm for strut and contrast in GLCM, which showed the highest AUC in each group, and FD are shown in Figure 9.

Table 5. Performance validation of strut and textural features using area under the curve (AUC), sensitivity and specificity in ROI 4.

Textural feature	AUC	95% CI	Sensitivity (%)	Specificity (%)	Accuracy (%)
FD	0.975	0.962-0.987	89.4	96.5	92.9
Strut					
HDA/total area	0.650	0.599-0.701	42.3	87.2	64.7
Periphery/total area	0.889	0.857-0.921	76.7	95.2	85.9
Periphery/HDA	0.836	0.798-0.874	71.4	88.1	79.7
TSL/HDA	0.833	0.794-0.873	64.3	96.9	80.6
TSL/total area	0.873	0.838-0.908	76.7	91.6	84.1
N.Tm/sq cm	0.727	0.678-0.776	58.8	90.3	73.5
N.Tm/TSL	0.587	0.533-0.640	45.8	75.8	60.7
N.Tm/periphery	0.523	0.463-0.570	33.9	81.9	57.9
N.Tm/HDA	0.697	0.646-0.747	57.3	83.3	70.2
N.Nd/sq cm	0.663	0.612-0.715	41.0	92.1	66.5
N.Nd/TSL	0.870	0.835-0.906	81.9	84.1	83.0
N.Nd/periphery	0.869	0.834-0.903	75.8	91.2	83.4
N.Nd/HDA	0.686	0.636-0.732	50.7	86.3	68.5
N.Nd/N.Tm	0.926	0.901-0.950	87.7	85.5	86.5
GLCM					
Contrast	0.580	0.528-0.633	48.9	66.5	57.7
Correlation	0.535	0.481-0.588	33.5	77.5	55.5
Energy	0.512	0.459-0.566	22.9	82.4	52.6
Homogeneity	0.543	0.490-0.596	52.0	58.1	55.0

Abbreviations: HDA, area of high-density region; Periphery, the total number of pixels on the outer margin of the high-density region; TSL, total length of struts; N, number; Tm, Termini; Nd, Nodes; sq, square.

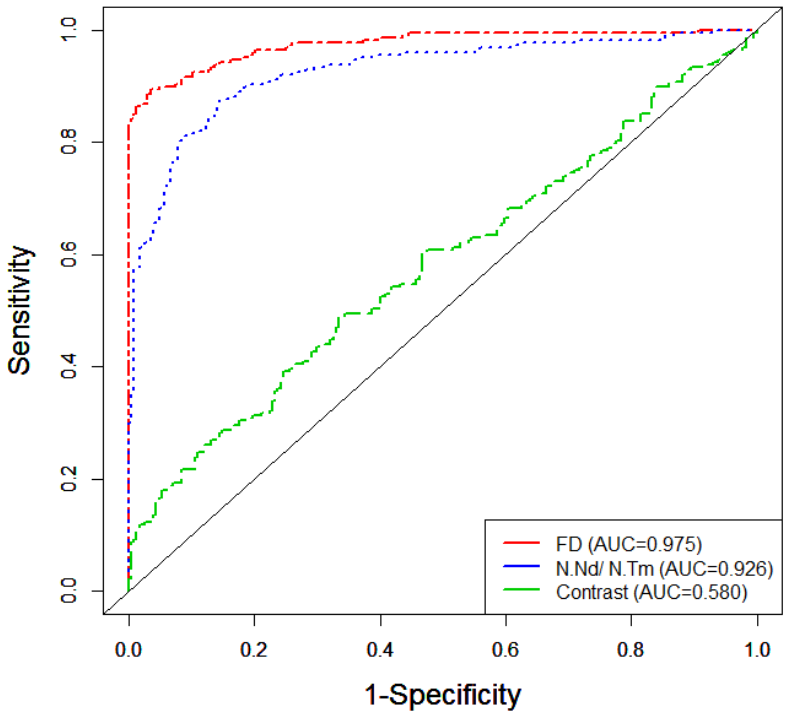

Figure 9. Receiver operating characteristic (ROC) curve of the fractal dimension (FD), N.Nd/N.Tm and contrast. FD and N.Nd/N.Tm showed excellent AUC for detecting osteoporosis over 0.9 whereas the AUC of GLCM showed low AUC around 0.5.

Abbreviations: N, number; Tm, Termini; Nd, Nodes.

The decision tree was composed of 4 decision nodes containing FD, N.Nd/N.Tm, and the number of nodes per square centimeter (N.Nd/sq cm) as well as 5 leaves that show the classification results (Fig 10). The accuracy of this classification tree was 89.1%, with 83.3% sensitivity and 95.4% specificity using 10-fold cross validation (Table 6).

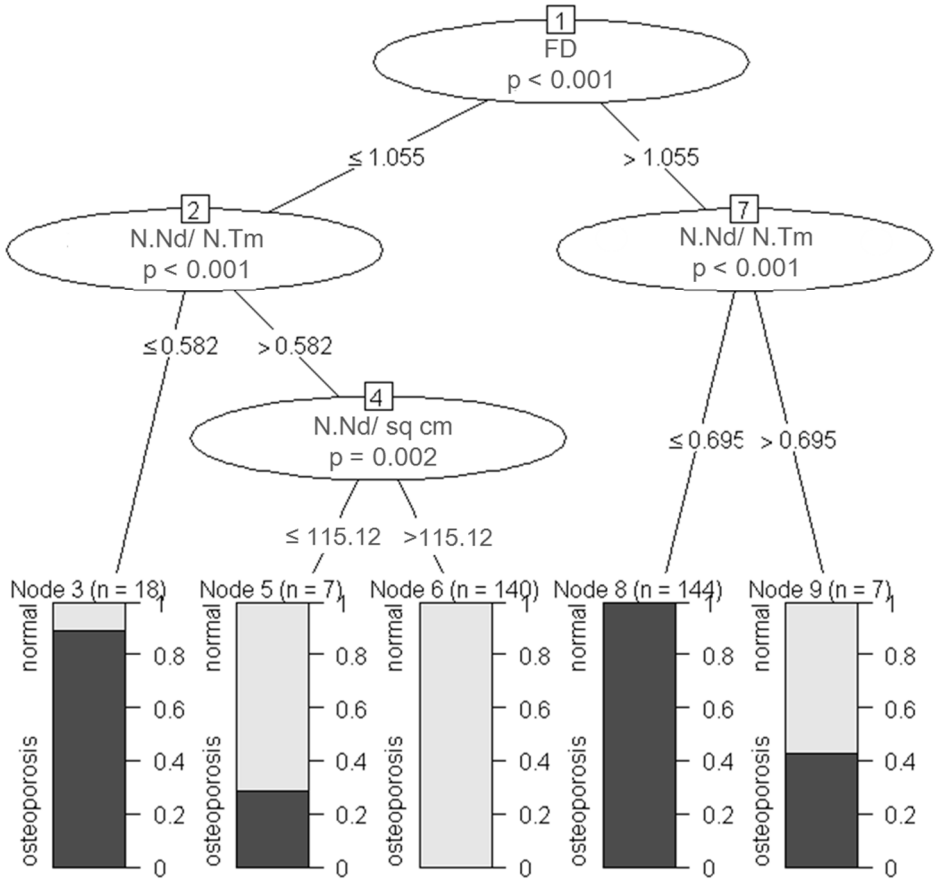

Figure 10. Decision tree algorithm performance identifying osteoporotic and normal patients. The decision tree was composed of fractal dimension (FD), N.Nd/N.Tm, and N.Nd/sq of the endosteal margin area, and displayed an accuracy of 89.1% for screening osteoporosis.

Abbreviations: N, number; Tm, Termini; Nd, Nodes; sq, square.

Table 6. Decision tree classification performance in 10-fold cross validation.

	Sensitivity	Specificity	Accuracy
Mean (10-fold)	0.833	0.950	0.891

IV. DISCUSSION

Many studies have analyzed the usefulness of DPRs as a screening tool for osteoporosis using visual assessment. Of these methods, MCI was generally accepted as a useful tool for osteoporosis screening.[27] This study tried to supplement the subjectivity of MCI by analyzing the strut, FD, and GLCM features of the endosteal margin area instead of visual assessment. We designed the new ROI 4, which includes both the inferior cortex and the marrow enclosing the endosteal margin, because erosive changes in osteoporotic patients appear in a broad area around the margin as a continuum. Three marrow areas were also analyzed using the combination of the above morphometric and texture features for exploring other useful ROIs and variables.

Strut analysis is a method of quantitative morphologic analysis that has been widely used to quantify structural elements in various objects in the medical field, including trabecular pattern analysis.[20,28-30] In dentistry, many studies have attempted to use this method to screen for osteoporosis in periapical radiography after White et al.[4,7,26] first introduced this method. However, this method has not yet been applied to multiple ROIs in DPRs including the endosteal margin area.

This study found that almost all the strut features in the endosteal margin area showed statistically significant differences between osteoporotic and non-osteoporotic patients. The number of strut variables which showed statistical significance was almost double those of the medullary portion of periapical radiography, which has a higher resolution than DPRs.[26] By logistic regression,

N.Nd/N.Tm, one of the strut variables in the endosteal margin area, showed an AUC of 0.926, which is the second highest of the features examined. This strut variable alone showed a similar AUC to the combination of variables reported by Kavitha et al.[24] who reported an AUC of 0.947. In osteoporotic patients, the number of termini was smaller, whereas the number of nodes was greater. These differences in terminus and node number could be explained by the different radiographic findings in the 2 groups. Since the integrity of the endosteal margin area is intact in the DPRs of normal patients, many independent high-density particles are present, resulted in a greater number of termini and a smaller number of nodes. However, erosive changes in the endosteal margin in osteoporotic patients resulted in a breakdown of the integrity in DPRs, resulting in wavy structures that have a longer than normal appearance, and correspond to a decrease in termini.

A number of studies have reported that FD could be useful in identifying osteoporosis in DPRs. In some studies[16,31], bone texture as captured by FD discriminated the presence of osteoporosis, whereas other studies reported no such relationship.[22,32,33] The AUC of FD in this study (0.975) showed that the diagnostic performance of FD at the endosteal margin area was excellent for osteoporosis screening. This result is higher than the AUC values of 0.857, 0.81, and 0.720 reported by Kavitha et al.[24], Oliveira et al.[34], and Roberts et al.[15], respectively. Many studies have reported a decrease in FD in osteoporotic patients in DPRs,[15,16,21,35] although a previous study reported a different result.[36] The FD of this study was higher in osteoporotic patients. The main cause for this disagreement may be the

difference in the ROI and variations in image quality, such as noise and the presence of overlapping structures.

The high AUC of strut features and FD of this study can be explained as due to several reasons. One reason maybe that we compared normal and osteoporotic patients without including patients with osteopenia. It might be confusing and difficult to find significant variables if ambiguous findings such as osteopenia are included. Our simple study design was hoped to allow us to find features that can distinguish between these 2 groups. Additionally, the endosteal margin area showed a high classification performance for detecting osteoporosis using objective features. The curved ROI of the customized program allowed it to focus on the margin area, which could not be analyzed properly using rectangular ROI forms. Third, larger sample size than previous studies may contribute to a high AUC statistically. Finally the upsampling strategy with parameter adjustment improved the image processing accuracy. By upsampling, ambiguous objects in the shadow area of an original image appeared clearly in a density-corrected image. This process resulted in the preservation of detailed structures of the binary and skeletonized images, which led to an improved capture of the morphologic and textural differences.

The GLCM is a statistical method for texture analysis using gray levels, but it has been used less frequently in the analysis of bone structure. A previous study reported that FD performed better than GLCM features.[24] Another study reported that GLCM outperformed FD for osteoporosis detection.[15] Contrast and homogeneity in the endosteal margin area of this study showed statistically

significant differences, but the AUC of these GLCM features were the lowest that we observed in this study (0.580). This result is lower than the AUC values of 0.733 and 0.824 reported in the previous studies of Kavitha et al.[24] and Roberts et al.[15] Their results are not directly comparable to this study due to differences in the ROI and calculation method. Unlike other studies that calculated the combined AUC of GLCM features, the AUC of GLCM in this study was calculated separately when evaluating the performance of each variable.

Few morphometric and textural variables showed statistical significance in ROIs 1-3, which cover the marrow area in DPRs. This result is consistent with that of a previous study, which reported that FD was not different in the medullary portion between the 2 groups[16], although other studies have reported opposite results.[21,37] Ghost images and overlapping structures such as the soft palate and airway might be one possible reason for this. Our results allow us to infer that the presence of erosive changes in the endosteal margin area in osteoporotic patients, instead of a medullary pattern, can be accurately analyzed by this objective analysis method in DPRs.

The decision tree comprised of FD, N.Nd/N.Tm, and N.Nd/sq cm of the endosteal margin area exhibited 89.1% accuracy for screening osteoporosis, which is similar to the 93.0% accuracy reported in the recent study of Kavitha et al.[24]. Our tree model also showed both a high sensitivity of 83.3% and a specificity of 95.4%, proving its high diagnostic power for detecting osteoporosis. This result shows that combination of these 3 variables in the endosteal margin area is an important

potential biomarker that can be used as an index (ODI) for supporting the early diagnosis of osteoporosis.

The major limitation of this study is that it used basic information, such as BMD, for screening osteoporosis. Further study is needed to co-analyze the effects of social factors such as the extent of smoking, alcohol consumption, amount of exercise, and nutritional supplements on DPRs in order to improve the accuracy of this method. This study did not include patients with in order to make the analysis clearer. Therefore, another challenge for our ODI will be to conduct another study to determine whether it can accurately discriminate among normal, osteopenic, and osteoporotic patients. This study used a larger number of subjects than other studies. However, 554 patients may be insufficient to generalize our ODI. Therefore, a study with massive amounts of data is needed to verify our ODI for clinical purposes. Furthermore, exploring the endosteal margin area in cone-beam computed tomography images with a 3-dimensional version of our index would also be an interesting project.

V. CONCLUSION

This study demonstrated that the endosteal margin area was an effective ROI that showed statistically significant differences in FD and most strut variables between osteoporotic and non-osteoporotic patients, whereas the medullary portion of DPRs showed few distinguishing features. We also found that the FD and strut variables showed high AUC values, while GLCM showed a low AUC. Additionally, the use of 2 strut features combined with FD in this area showed high diagnostic performance in screening osteoporotic patients from the normal group. Our findings suggest that the combination of these 3 variables in the endosteal margin area has a great potential as an index (ODI) for the early detection of osteoporosis.

REFERENCES

1. Consensus development conference: diagnosis, prophylaxis, and treatment of osteoporosis. Am J Med 1993;94:646-50.
2. Yu B, Wang CY. Osteoporosis: The Result of an 'Aged' Bone Microenvironment. Trends Mol Med 2016; doi:10.1016/j.molmed.2016.06.002.
3. Cummings SR, Melton LJ. Epidemiology and outcomes of osteoporotic fractures. Lancet 2002;359:1761-7.
4. White SC, Atchison KA, Gornbein JA, Nattiv A, Paganini-Hill A, Service SK, et al. Change in mandibular trabecular pattern and hip fracture rate in elderly women. Dentomaxillofac Radiol 2005;34:168-74.
5. Hernlund E, Svedbom A, Ivergard M, Compston J, Cooper C, Stenmark J, et al. Osteoporosis in the European Union: medical management, epidemiology and economic burden. A report prepared in collaboration with the International Osteoporosis Foundation (IOF) and the European Federation of Pharmaceutical Industry Associations (EFPIA). Arch Osteoporos 2013;8:136.
6. Office of the Surgeon G. Reports of the Surgeon General. Bone Health and Osteoporosis: A Report of the Surgeon General. Rockville (MD): Office of the Surgeon General (US); 2004.

7. Lee BD, White SC. Age and trabecular features of alveolar bone associated with osteoporosis. Oral Surg Oral Med Oral Pathol Oral Radiol Endod 2005;100:92-8.

8. Hildebolt CF. Osteoporosis and oral bone loss. Dentomaxillofacial Radiology 1997;26:3-15.

9. von Wowern N, Klausen B, Kollerup G. Osteoporosis: a risk factor in periodontal disease. Journal of Periodontology 1994;65:1134-8.

10. Civitelli R, Pilgram T, Dotson M, Muckerman J, Lewandowski N, Armanmento-Villareal R. Hormone/estrogen replacement therapy improves alveolar and postcranial bone density in postmenopausal women: A randomized, double-blind, placebo-controlled trial. Archives of Internal Medicine 2002.

11. Payne JB, Reinhardt RA, Nummikoski PV, Patil KD. Longitudinal alveolar bone loss in postmenopausal osteoporotic/osteopenic women. Osteoporosis International 1999;10:34-40.

12. Steiner E, Jergas M, Genant HK. Radiology of osteoporosis. Osteoporosis 1996:1019-54.

13. Bollen AM, Taguchi A, Hujoel PP, Hollender LG. Case-control study on self-reported osteoporotic fractures and mandibular cortical bone. Oral Surgery, Oral Medicine, Oral Pathology, Oral Radiology, and Endodontics 2000;90:518-24.

14. Taguchi A, Suei Y, Ohtsuka M, Otani K, Tanimoto K, Ohtaki M. Usefulness of panoramic radiography in the diagnosis of postmenopausal

osteoporosis in women. Width and morphology of inferior cortex of the mandible. Dentomaxillofacial Radiology 1996;25:263-7.

15. Roberts MG, Graham J, Devlin H. Image texture in dental panoramic radiographs as a potential biomarker of osteoporosis. IEEE Trans Biomed Eng 2013;60:2384-92.

16. Sindeaux R, Figueiredo PT, de Melo NS, Guimaraes AT, Lazarte L, Pereira FB, et al. Fractal dimension and mandibular cortical width in normal and osteoporotic men and women. Maturitas 2014;77:142-8.

17. Hardanti S, Azhari, Oscandar F. Description of mandibular bone quality based on measurements of cortical thickness using Mental Index of male and female patients between 40-60 years old. Imaging Sci Dent 2011;41:151-3.

18. Lopez-Lopez J, Estrugo-Devesa A, Jane-Salas E, Ayuso-Montero R, Gomez-Vaquero C. Early diagnosis of osteoporosis by means of orthopantomograms and oral x-rays: a systematic review. Med Oral Patol Oral Cir Bucal 2011;16:e905-13.

19. Klemetti E, Kolmakov S, Kröger H. Pantomography in assessment of the osteoporosis risk group. Scandinavian Journal of Dental Research 1994;102:68-72.

20. Law AN, Bollen AM, Chen SK. Detecting osteoporosis using dental radiographs: A comparison of four methods. Journal of the American Dental Association 1996;127:1734-42.

21. Koh KJ, Park HN, Kim KA. Prediction of age-related osteoporosis using fractal analysis on panoramic radiographs. Imaging Sci Dent 2012;42:231-5.

22. Tosoni GM, Lurie AG, Cowan AE, Burleson JA. Pixel intensity and fractal analyses: detecting osteoporosis in perimenopausal and postmenopausal women by using digital panoramic images. Oral Surg Oral Med Oral Pathol Oral Radiol Endod 2006;102:235-41.

23. Yasar F, Akgunlu F. The differences in panoramic mandibular indices and fractal dimension between patients with and without spinal osteoporosis. Dentomaxillofac Radiol 2006;35:1-9.

24. Kavitha MS, An SY, An CH, Huh KH, Yi WJ, Heo MS, et al. Texture analysis of mandibular cortical bone on digital dental panoramic radiographs for the diagnosis of osteoporosis in Korean women. Oral Surg Oral Med Oral Pathol Oral Radiol 2015;119:346-56.

25. White SC, Taguchi A, Kao D, Wu S, Service SK, Yoon D, et al. Clinical and panoramic predictors of femur bone mineral density. Osteoporos Int 2005;16:339-46.

26. White SC, Rudolph DJ. Alterations of the trabecular pattern of the jaws in patients with osteoporosis. Oral Surg Oral Med Oral Pathol Oral Radiol Endod 1999;88:628-35.

27. Calciolari E, Donos N, Park JC, Petrie A, Mardas N. Panoramic measures for oral bone mass in detecting osteoporosis: A systematic review and meta-analysis. Journal of Dental Research 2015;94:17S-27S.

28. Croucher PI, Garrahan NJ, Compston JE. Assessment of cancellous bone structure: comparison of strut analysis, trabecular bone pattern factor, and marrow space star volume. J Bone Miner Res 1996;11:955-61.

29. Schmah T, Marwan N, Thomsen JS, Saparin P. Long range node-strut analysis of trabecular bone microarchitecture. Med Phys 2011;38:5003-11.

30. Uchiyama T, Tanizawa T, Ito A, Endo N, Takahashi HE. Microstructure of the trabecula and cortex of iliac bone in primary hyperparathyroidism patients determined using histomorphometry and node-strut analysis. J Bone Miner Metab 1999;17:283-8.

31. Yasar F, Akgunlu F. Evaluating mandibular cortical index quantitatively. Eur J Dent 2008;2:283-90.

32. Mohajery M, Brooks SL. Oral radiographs in the detection of early signs of osteoporosis. Oral Surgery, Oral Medicine, Oral Pathology 1992;73:112-7.

33. Yaşar F, Akgünlü F. The differences in panoramic mandibular indices and fractal dimension between patients with and without spinal osteoporosis. Dentomaxillofacial Radiology 2006;35:1-9.

34. Alman AC, Johnson LR, Calverley DC, Grunwald GK, Lezotte DC, Hokanson JE. Diagnostic capabilities of fractal dimension and mandibular cortical width to identify men and women with decreased bone mineral density. Osteoporos Int 2012;23:1631-6.

35. Oliveira ML, Pedrosa EF, Cruz AD, Haiter-Neto F, Paula FJ, Watanabe PC. Relationship between bone mineral density and trabecular bone pattern in

postmenopausal osteoporotic Brazilian women. Clin Oral Investig 2013;17:1847-53.

36. Bollen AM, Taguchi A, Hujoel PP, Hollender LG. Fractal dimension on dental radiographs. Dentomaxillofac Radiol 2001;30:270-5.

37. Aranha Watanabe PC, Moreira Lopes De Faria L, Mardegan Issa JP, Caldeira Monteiro SA, Tiossi R. Morphodigital evaluation of the trabecular bone pattern in the mandible using digitized panoramic and periapical radiographs. Minerva Stomatol 2009;58:73-80.

Abstract (Korean)

Strut와 텍스쳐 분석을 통해 파노라마에서 골다공증을 검출하는 지수 (index)의 개발

황재준

연세대학교 대학원 치의학과

(지도교수 한상선)

전 세계 인구의 빠른 노령화와 함께, 골다공증을 예측하고 조기 진단하는 것은 중요한 보건 이슈가 되었다. 이 연구의 목적은 파노라마에서 골내막 경계부 (endosteal margin area)를 포함한 여러 개의 관심영역에서 스트러트 분석 (strut analysis), 프랙탈 차원 (fractal dimension, FD) 및 회색조 동시발생 매트릭스 (gray level co-occurrence matrix, GLCM)를 이용하여 골다공증을 진단할 수 있는 변수를 찾고, 이를 통해 파노라마를 이용한 골다공증 검출 지수 (ODI)을 개발하는 것이다.

2012년부터 2015년까지 연세대학교 치과 병원을 내원한 환자 중 골밀도 지수 (T score)로 정상 및 골다공증으로 분류된 각각 272명씩, 총 454명의 파노라마 사진이 이용되었다. 세 군데의 수질골 부위와 endosteal margin 영역이 400%로 업샘플링 (upsampling)된 후, 스트러트 변수, FD, 그리고 GLCM 이 직접 제작한 이미지 처리 프로그램에 의해 분석되었다. 독립 표본 t검정 (independent samples t-test)은 정상과 골다공증 환자군 사이의 통계적인 차이를 검증하기 위해 사용되었다. 각각의 변수들의 진단 정확성을 비교하기 위해 로지스틱 회귀분석 (logistic regression)이 사용되었다. 마

지막으로, 골다공증 검출 지수(ODI)를 만들고 검증하기 위해 판단 트리(decision tree)가 사용되었다.

골내막 경계부의 FD (0.975)와 스트러트 변수들 (0.926 이하)은 높은 곡선 하면적 (area under the curve, AUC) 값을 보인 반면, GLCM (0.580 이하)은 낮은 AUC 값을 보였다. FD와 두 스트러트 변수들 (교점의 수를 종점의 수로 나눈 값, 그리고 1 평방 센티미터 당 교점의 수)의 조합은 결정 트리 방법을 사용하여 높은 진단 정확도 (89.1%)를 보여주었다.

골내막 경계부의 FD와 두 strut 변수의 조합은 파노라마에서 골다공증 검출 지수 (ODI)로써의 가능성을 보여주었다.

중심단어: 프랙탈; 이미지 프로세싱; 하악; 골다공증; 방사선학